MOLECULAR BIOLOGY

Human POT1 protects the telomeric ds-ss DNA junction by capping the 5' end of the chromosome

Valerie M. Tesmer, Kirsten A. Brenner, Jayakrishnan Nandakumar*

Protection of telomeres 1 (POT1) is the 3' single-stranded overhang-binding telomeric protein that prevents an ataxia telangiectasia and Rad3-related (ATR) DNA damage response (DDR) at chromosome ends. What precludes the DDR machinery from accessing the telomeric double-stranded-single-stranded junction is unknown. We demonstrate that human POT1 binds this junction by recognizing the phosphorylated 5' end of the chromosome. High-resolution crystallographic structures reveal that the junction is capped by POT1 through a "POT-hole" surface, the mutation of which compromises junction protection in vitro and telomeric 5'-end definition and DDR suppression in human cells. Whereas both mouse POT1 paralogs bind the single-stranded overhang, POT1a, not POT1b, contains a POT-hole and binds the junction, which explains POT1a's sufficiency for end protection. Our study shifts the paradigm for DDR suppression at telomeres by highlighting the importance of protecting the double-stranded-single-stranded junction.

ucleoprotein complexes called telomeres cap chromosome ends to ensure genome integrity. Human telomeric DNA contains ~10 to 15 kb of tandem 5'-GGTTAG-3'/3'-CCAATC-5' repeats. Although telomeric DNA is primarily double-stranded (ds), all chromosomes terminate in a 50- to 500nucleotide (nt) single-stranded (ss) G-rich telomeric overhang (Fig. 1A, bottom) (1). The six-protein shelterin complex coats telomeric DNA to protect chromosome ends from being recognized as dsDNA breaks by the ataxia telangiectasia and Rad3-related (ATR) kinaseand ataxia-telangiectasia mutated (ATM) kinase-mediated DNA damage response (DDR) machineries (2, 3). ATR signaling involves multiple protein factors and coordinated recognition of both the ss and the adjacent ds-ss junction of its DNA substrates (4). Protection of telomeres 1 (POT1) is a shelterin component that binds the ss G-rich overhang with high affinity and sequence specificity and prevents ATR signaling at telomeres (2, 5, 6). POT1 recognizes ssDNA through its DNA binding domain (DBD), which consists of two oligonucleotide/oligosaccharide-binding (OB) domains (Fig. 1A). Previous studies have reported a decanucleotide TTAGGGTTAG within two telomeric ss repeats, ¹GGTTAGGGTTAG¹², to be sufficient for high-affinity binding to human POT1 (hPOT1) (7). The first OB domain (OB1) of hPOT1 binds ³TTAGGG⁸ (OB1^{DNA}), whereas its second OB domain (OB2) binds ⁹TTAG¹² (OB2^{DNA}) (Fig. 1, A and B) (7). Homologs of POT1 are identifiable across eukarvotes (5, 8-15), and deleting the POT1 paralog in mice that is involved in chromosome-end protection (POT1a) is embryonic lethal (14, 15).

Department of Molecular, Cellular and Developmental Biology, University of Michigan, Ann Arbor, MI 48109, USA. *Corresponding author. Email: jknanda@umich.edu

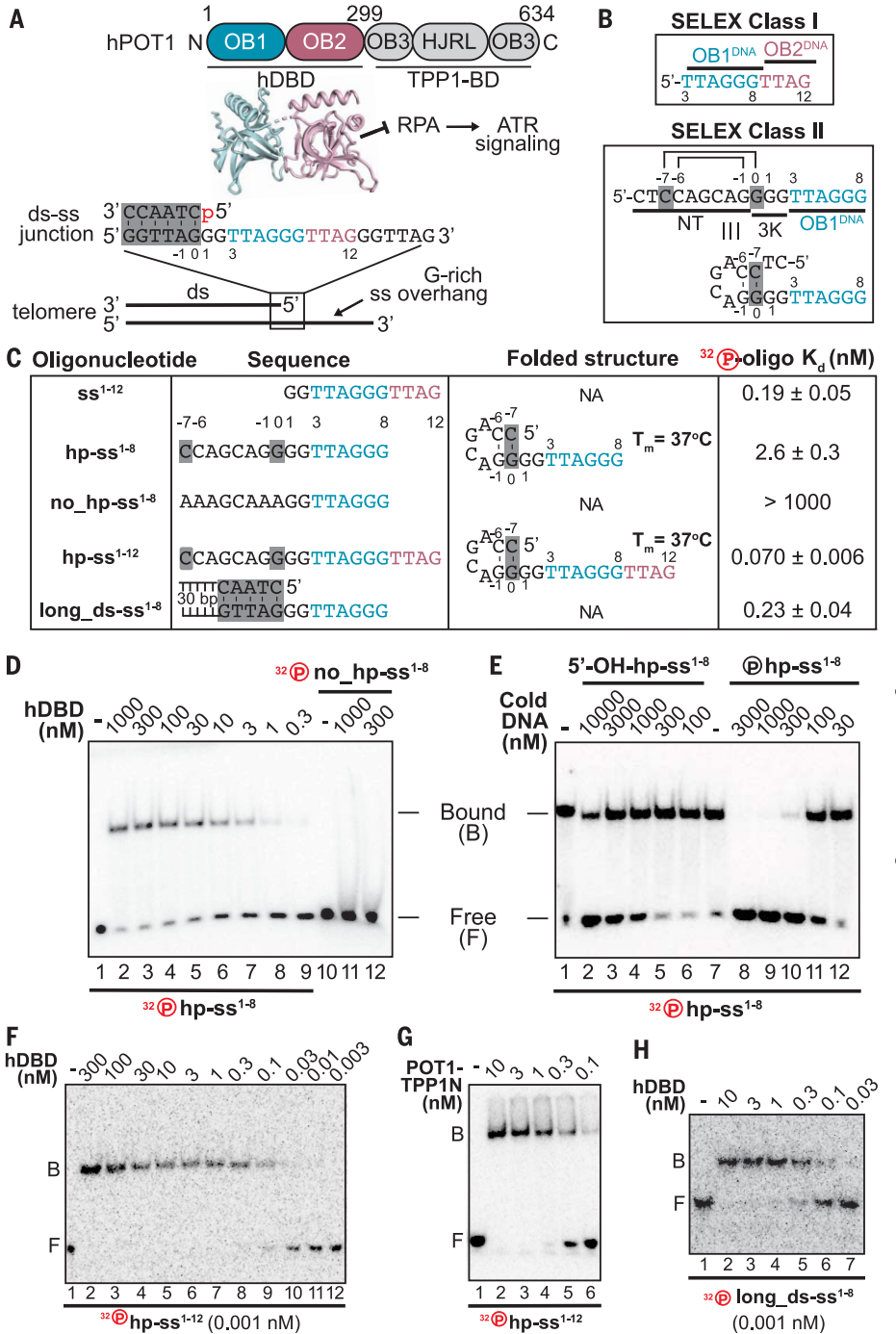
The current model for ATR suppression at telomeres invokes the prevention by POT1 of replication protein A (RPA) loading onto the ss overhang, through POT1's high affinity for telomeric ssDNA and its tethering to the rest of shelterin at telomeric dsDNA (2, 6, 16). Yet, multiple observations suggest that additional features of POT1 are involved in ATR repression. First, mouse POT1 paralogs POT1a and POT1b display indistinguishable ssDNAbinding activity, but only POT1a is sufficient for chromosome-end protection (6, 15, 17), whereas POT1b regulates chromosome-end processing and replication activities (16, 18-21). Replacing the DBD of POT1b with that of POT1a or hPOT1 enables ATR repression at telomeres (17). Second, replacing the DBD of POT1a with that of ssDNA-binding protein RPA70 is not sufficient to fully repress ATR signaling at telomeres in mouse cells that lack POTIa (16). Moreover, POT1's binding to the G-rich ss overhang does not explain how it dictates the 5' end of the C-rich strand, which terminates predominantly in ATC-5' in mammals (22, 23) (Fig. 1A, bottom). These observations are consistent with the DBD of hPOT1 and mouse POT1a carrying out an additional function relevant to ATR suppression.

Human POT1 binds a 5'-phosphorylated telomeric ds-ss DNA junction

We hypothesized that hPOT1 binds to the telomeric ds-ss junction after we reanalyzed its published DNA binding-site preferences. Two classes of POT1 binding sites emerged from previous SELEX (systematic evolution of ligands by exponential enrichment) analysis, one of which was the expected $^3\mathrm{TTAGGGTTAG^{12}}$ (OB1 $^\mathrm{DNA}$ and OB2^{DNA}) site (Fig. 1B, Class I) (24). A second class contained OB1^{DNA}, an upstream tri-K ("K" indicates a G or T nucleotide), and a seemingly nontelomeric (NT) sequence implicated in binding

to OB1 (consensus: CTCCAGCAGGGGTTTAG Check for (Fig. 1B, Class II) (24). Junction binding suspected on the basis of the observation that the tri-K GGG motif corresponds to the telomeric repeat sequence upstream of OBI^{DNA}, and NT sequences in the Class II hits could fold into a hairpin (hp) containing a 2-base-pair (bp) stem ⁻¹GG⁰/⁻⁶CC⁻⁷ and a variable tetraloop (positions -5 to -2) (Fig. 1B and fig. S1, A and B). In this interpretation, G⁰ and C⁻⁷ represent the first base pair at the ds-ss junction (with C^{-7} corresponding to the 5' end of the mammalian chromosome), and the 3' overhang initiates in the GGTTAG register (Fig. 1, A and B, and fig. S1, A and B). We conducted a quantitative electrophoretic mobility shift assay (EMSA) with purified hPOT1 DBD (hDBD) (fig. S2A) and a 5'-32Plabeled hp oligonucleotide derived from the Class II consensus terminating in a C at the 5' end and containing a 3' overhang of sequence $^1\!GGTTAGGG^8$ (hp-ss $^{1-8}$) (Fig. 1C). The absence of OB2 DNA from the Class II consensus attenuates the affinity of hDBD for ssDNA (7), allowing us to assess DNA affinity of POT1 for the ds-ss junction. hDBD bound strongly to hp-ss¹⁻⁸ [dissociation constant (K_d) = 2.6 ± 0.3 nanomolar (nM)] but not to a similar target (no_hp-ss¹⁻⁸) that lacks the ability to form a hairpin (Fig. 1, C and D). The natural telomeric ds-ss junction ends in a 5'-phosphate (5'-P), which has been previously exploited to determine the 5'-terminal nt of chromosomes by using DNA ligasemediated methods (25). To test the importance of this phosphate in binding hPOT1, we performed a competition experiment mixing 5'-³²P-hp-ss¹⁻⁸ with either nonradiolabeled 5'-phosphorylated hp-ss¹⁻⁸ or 5'-OH-hp-ss¹⁻⁸ before binding to hDBD. The 5'-P was required to effectively outcompete POT1 binding to the radiolabeled DNA (Fig. 1E). The absence of a 5'-P at the DNA junction in past in vitro studies may have prevented the detection of this previously unappreciated POT1 DNAbinding activity (17, 26-29). POT1 bound to a telomeric ds-ss junction in vivo is poised to engage both OB1DNA and OB2DNA. Extension of the overhang of the hp to include OB2^{DNA} (hp- $\mathrm{ss^{1\text{-}12}})$ resulted in a higher affinity for hDBD $[K_d = 70 \text{ picomolar (pM)}]$ (Fig. 1, C and F) compared with either ss¹⁻¹² ($K_d = 190 \text{ pM}$) (Fig. 1C and fig. S2B) or hp-ss¹⁻⁸ (Fig. 1, C and D). We confirmed that a heterodimer of full-length hPOT1 and shelterin partner TINT1-PTOP-PIP1 (TPP1) (by using the TPP1N truncation construct), which approximates the context of hPOT1 coating the ss overhang in vivo (30, 31), exhibited robust binding to 5'-P-hp-ss1-12 (Fig. 1G). DBD bound a two-stranded DNA (duplex reinforced with 30 bp of arbitrary, nontelomeric sequence) terminating in 5 bp of native ds telomeric junction sequence and an 8-nt overhang (long_ds-ss¹⁻⁸) with an affinity that was approximately one order of magnitude greater than observed with hp-ss¹⁻⁸, likely

Fig. 1. Human POT1 recognizes the 5'-phosphorylated ds-ss junction of telomeres. (A) (Top) Schematic of hPOT1 includes binding domains for ssDNA (hDBD) and TPP1 (TPP1-BD). hDBD (PDB: 1XJV) is composed of OB1 and OB2. The current model suggests that POT1 outcompetes the ssDNA-binding RPA complex to prevent ATR signaling at telomeres. HJRL, Holliday junction resolvase-like. (Bottom) Mammalian chromosomes end in a ds-ss junction containing ATC-5' (predominantly) and a ss G-rich overhang. Numbering starts with the first overhang nucleotide. (B) A previous SELEX study revealed two hPOT1-binding DNA classes (24). Class I harbors the known sites for OB1 and OB2, denoted as OB1^{DNA} (cyan) and OB2^{DNA} (pink), respectively. Class II revealed a consensus containing a seemingly nontelomeric (NT) sequence upstream of OB1^{DNA} that can potentially fold into a hp: "K" indicates a G or T nucleotide and the shaded area indicates the sequence of the first bp at the telomeric ds-ss junction. (C) Annotated name, sequence, predicted hp structure [with $T_{\rm m}$ (where $T_{\rm m}$ is the temperature at which 50% of dsDNA is denatured) calculated by the UNAFold web server], and mean K_d and SD (of binding to hDBD) of the oligonucleotides used in EMSA analysis. NA indicates not applicable. (D to H) EMSA of indicated proteins (hDBD or POT1-TPP1N heterodimer) and 5'-32P-labeled DNA oligonucleotides. (D), (F), (G), and (H) indicate direct binding experiments, and (E) indicates a competition experiment. In (D). 0.1 nM 5'-32P-hp-ss¹⁻⁸ was used: the number of experimental replicates n = 5 for hp-ss¹⁻⁸ (full and partial titrations); n = 3 for no hp-ss¹⁻⁸. In (E), 100 nM hDBD and 0.1 nM 5'-32P-labeled hp-ss1-8 were incubated with indicated amounts of unlabeled hp-ss¹⁻⁸ (cold DNA) containing either a 5'-OH or a 5'-P; n = 3. In (F), 0.001 nM 5'-³²P-hp-ss¹⁻¹² was used; n = 3. In (G), 0.01 nM 5'-³²P-hp-ss¹⁻¹² was used; n = 3. (H) 0.001 nM 5'- 32 P-long_ds-ss $^{1-8}$ was used; n = 3. Circled red "P" indicates radiolabeled; circled black "P" indicates nonradiolabeled. Bound (B) indicates DNA bound to protein; Free (F) indicates free, unbound DNA.



reflecting the greater stability of the more physiologically representative duplex DNA versus that of the hp (Fig. 1, C and H). Our data demonstrate that the telomeric ds-ss junction is a previously unappreciated high-affinity binding site for hPOT1.

High-resolution structures reveal how human POT1 caps the phosphorylated 5' end of a telomeric junction

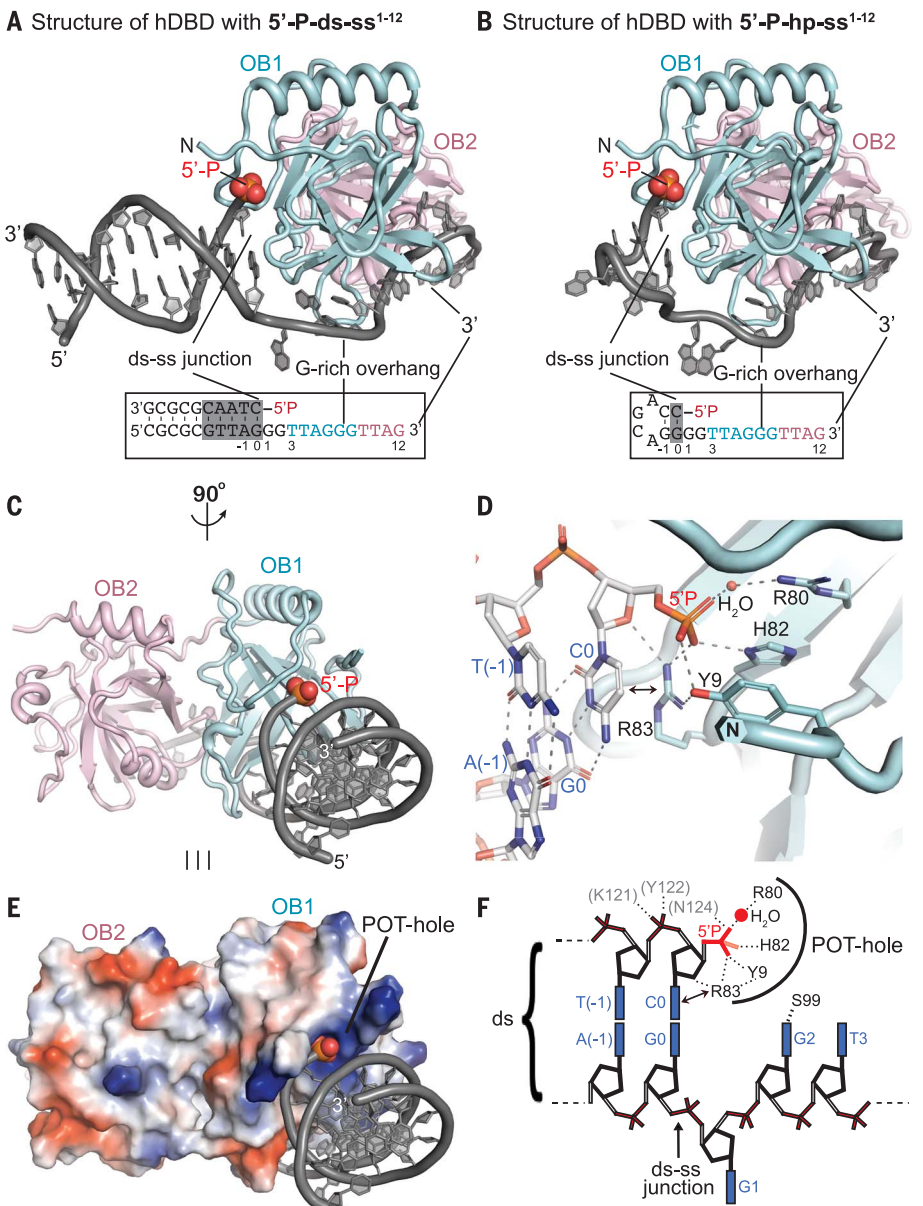
To determine the structural basis for hPOTI's telomeric ds-ss junction-binding activity, we

formed complexes of hDBD with two substrates that mimic the telomeric ds-ss junction—5′-P-ds-ss¹-¹² (DNA containing a 5-bp arbitrary, nontelomeric tether upstream of GTTAG/CAATC-5′-P native telomeric ds sequence extending into a 12-nt 3′ overhang) (fig. S2, C and D) and 5′-P-hp-ss¹-¹² (Fig. 1C)—and solved their structures using x-ray crystallography (Fig. 2, A and B). The hDBD-bound 5′-P-ds-ss¹-¹² and 5′-P-hp-ss¹-¹² structures were solved to 2.60- and 2.16-Å resolution, respectively (table S1). Both structures are similar to each other (fig. S3D) and

recapitulate the previously reported hDBD-ss DNA-binding interface with minor differences (fig. S3, A to C, and E to J) (7). These structures reveal how hPOT1 binds the phosphorylated 5' end of the telomeric ds-ss junction (Fig. 2). An electropositive pocket of four amino acids (Y9, R80, H82, and R83) in the hPOT1 OB1 domain that we name the "POT-hole" caps the 5'-P-cytidine nucleotide by means of a network of stacking and electrostatic interactions (Fig. 2, D to F, and fig. S4A). R83 acts as the linchpin by forming an ionic interaction with the 5'-P,

Fig. 2. Structural basis of telomeric junction 5'- end protection by human POT1. (A and B)

Cartoon representation of high-resolution crystal structures of complexes of (A) hDBD with 5'-P-dsss¹⁻¹² and (B) 5'-P-hp-ss¹⁻¹², showing OB1 (cyan) and OB2 (pink) bound to DNA [gray, with the exception of the 5'-P, whose atoms are shown as spheres and in Corey-Pauling-Koltun (CPK) coloring] A boxed schematic of the DNA is shown below the structure, with the ds sequence found naturally at the telomeric ds-ss junction shaded gray, the 5'-P in red, and residues in the G-rich 3' overhang colored to indicate binding by OB1 and OB2, respectively. (C) Cartoon and (E) electrostatic surface (blue is electropositive and red is electronegative) representations of the hDBD-5'-P-ds-ss¹⁻¹² structure shown in a view orthogonal to that in (A). The 5'-P occupies a pocket in POT1 that is complementary in shape and charge. Single-letter abbreviations for the amino acid residues are as follows: H, His; R, Arg; and Y, Tyr. (D) The POT-hole-DNA interface within the hDBD-5'-P-hp-ss¹⁻¹² structure is shown with POT-hole side chains (carbon in cyan) and the nucleotides (carbon in light gray) near the junction shown as sticks. A water molecule bridging hPOT1 R80 to the 5'-P is shown as an orange sphere. The dashed lines indicate H-bonds and ionic interactions, the double-headed arrow indicates stacking of the hPOT1 R83 side chain with the 5'-C at the junction (numbered CO), and N indicates the N terminus of hDBD resolved in the crystal structure. (F) Interaction map of hDBD with the ds-ss junction.



stacking against the 5'-cytosine base, and forming hydrogen bonds (H-bonds) with the ribosering oxygen of the 5'-cytidine nucleoside (5'-C) (Fig. 2, D and F, and fig. S4A). R83 also forms an H-bond with Y9, which along with H82 interacts with the 5'-P. R80 forms a watermediated H-bond with the 5'-P. We observed that the POT-hole is not optimally sized to accommodate a bulkier adenine (purine instead of a pyrimidine) or thymine (methyl group on the base) at the 5' end because of steric clashes (fig. S5, A to C). Furthermore, the fixed distance between the POT-hole and the ssDNA-binding region of hPOT1 dictates the preference for the naturally occurring ATC-5' versus alternative 5'-C iterations: ATCC-5' and ATCCC-5' (fig. S5D). In addition to interactions involving the POThole, junction recognition is fortified by contacts made by the backbone amides of hPOT1 amino acids 121 to 124 with the phosphodiester group penultimate to the 5'-C (Fig. 2F and fig. S4B), as well as S99 with G² (Fig. 2F and fig. S3, K and L). These data provide the structural basis for binding of the telomeric ds-ss junction by hPOT1.

The POT-hole dictates telomeric DNA junction binding and inhibits DDR at telomeres

We evaluated the importance of the POT-hole in binding the telomeric ds-ss junction in vitro using purified hDBD variants with alanine mutations at Y9, R80, H82, and R83 (fig. S6A).

We also engineered an R83E charge-reversal mutant to test the importance of the ionic R83-5'-P interaction. Alanine substitution of F62, a residue in hPOT1 OB1 that is indispensable for binding telomeric ssDNA (32), was included as a control to disrupt binding to both ssDNA and the ds-ss junction. In agreement with the structural data, little to no DNA binding was observed for any POT-hole mutant with the 5'-P-hp-ss¹⁻⁸, even at concentrations 100-fold greater than the $K_{\rm d}$ with wild-type (WT) hDBD (Fig. 3A, left). By contrast, POT-hole mutants bound 5'-P-ss¹⁻¹² with an affinity similar to that of wild type (Fig. 3A, right, and fig S6, B and C). F62A failed to bind either oligonucleotide, which is consistent with binding to OB1DNA

ss G-rich overhang -

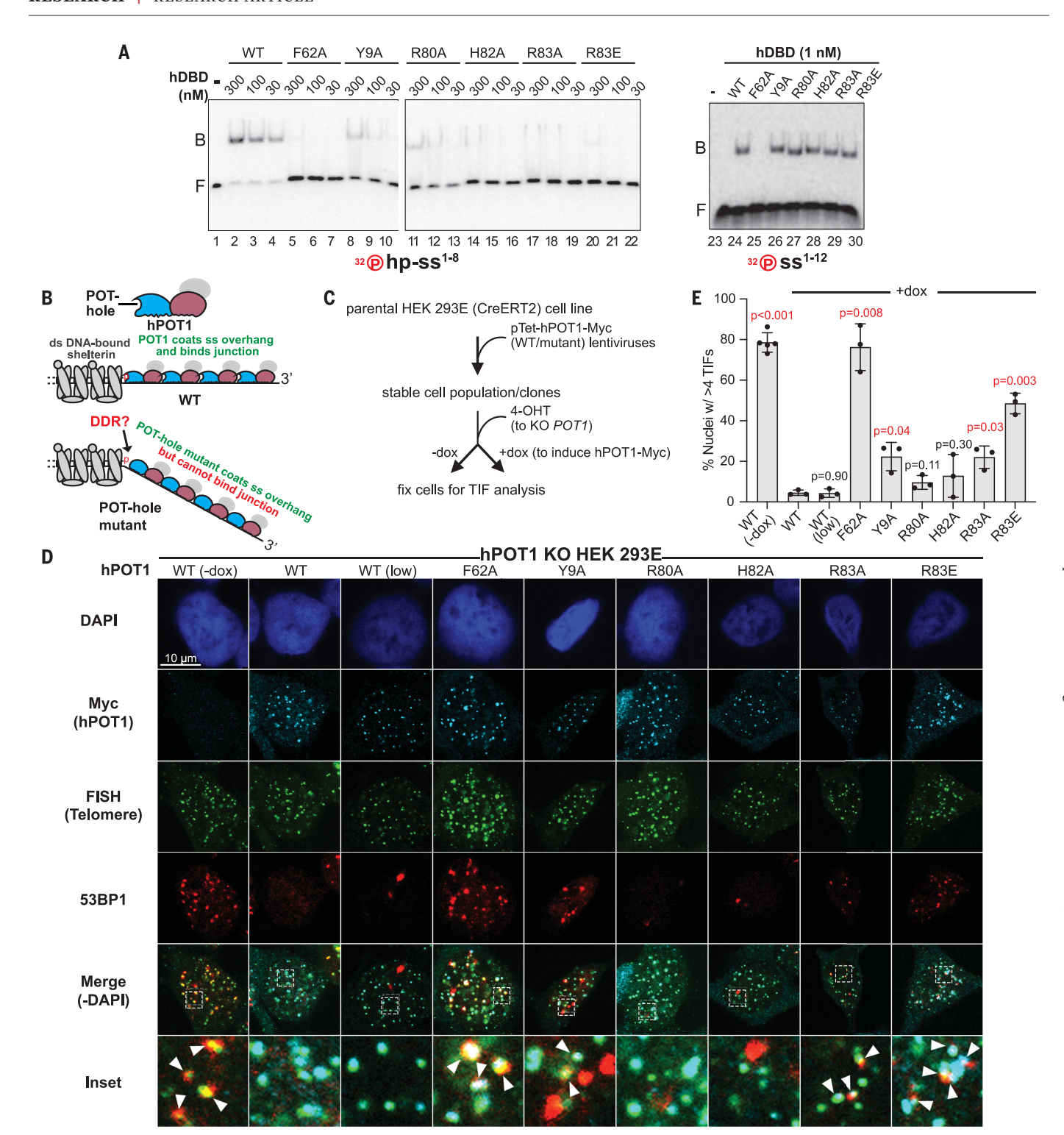


Fig. 3. Separation-of-function POT-hole mutations abrogate ds-ss DNA junction binding in vitro and result in a DDR at human telomeres.

(**A**) EMSA to detect direct binding of WT or indicated mutant hDBD constructs with 5'- 32 P-hp-ss¹⁻⁸ (0.1 nM; lanes 1 to 22) and 5'- 32 P-ss¹⁻¹² (0.1 nM; lanes 23 to 30); n=3. (**B**) Schematic conveying how POT-hole mutations would disrupt binding to the ds-ss junction but not coating of the ss overhang by POT1. (**C**) Scheme for deletion of endogenous *POT1* and complementation with lentivirally transduced hPOT1-Myc to assess the ability of mutants to suppress TIF formation in a HEK 293E-based cell line (*34*). (**D**) TIF analysis of cell lines after 4-OHT and dox (1000 ng/ml; 25 ng/ml in "low dox" wild type) treatment as described in (C) performed

with peptide nucleic acid fluorescent in situ hybridization (PNA-FISH) for telomeres (green) and immunofluorescence (IF) for Myc (hPOT1; cyan) and 53BP1 (red). 4',6-diamidino-2-phenylindole (DAPI) was used to stain the nucleus (blue). Overlap of the telomeric and 53BP1 foci (and Myc foci, if applicable) in the "Merge" panel indicates TIFs. (Inset) Magnified view of the boxed area within the image; arrowheads indicate TIFs. (E) Quantitation of TIF data of which (D) is representative. Mean and SD (n=3 for all conditions except WT –dox, for which n=5; each +dox set containing >75 nuclei and each –dox set containing >50 nuclei) for TIFs are plotted for the indicated cell lines. P values calculated with a two-tailed Student's t test for comparisons against WT +dox data are indicated above the bars.

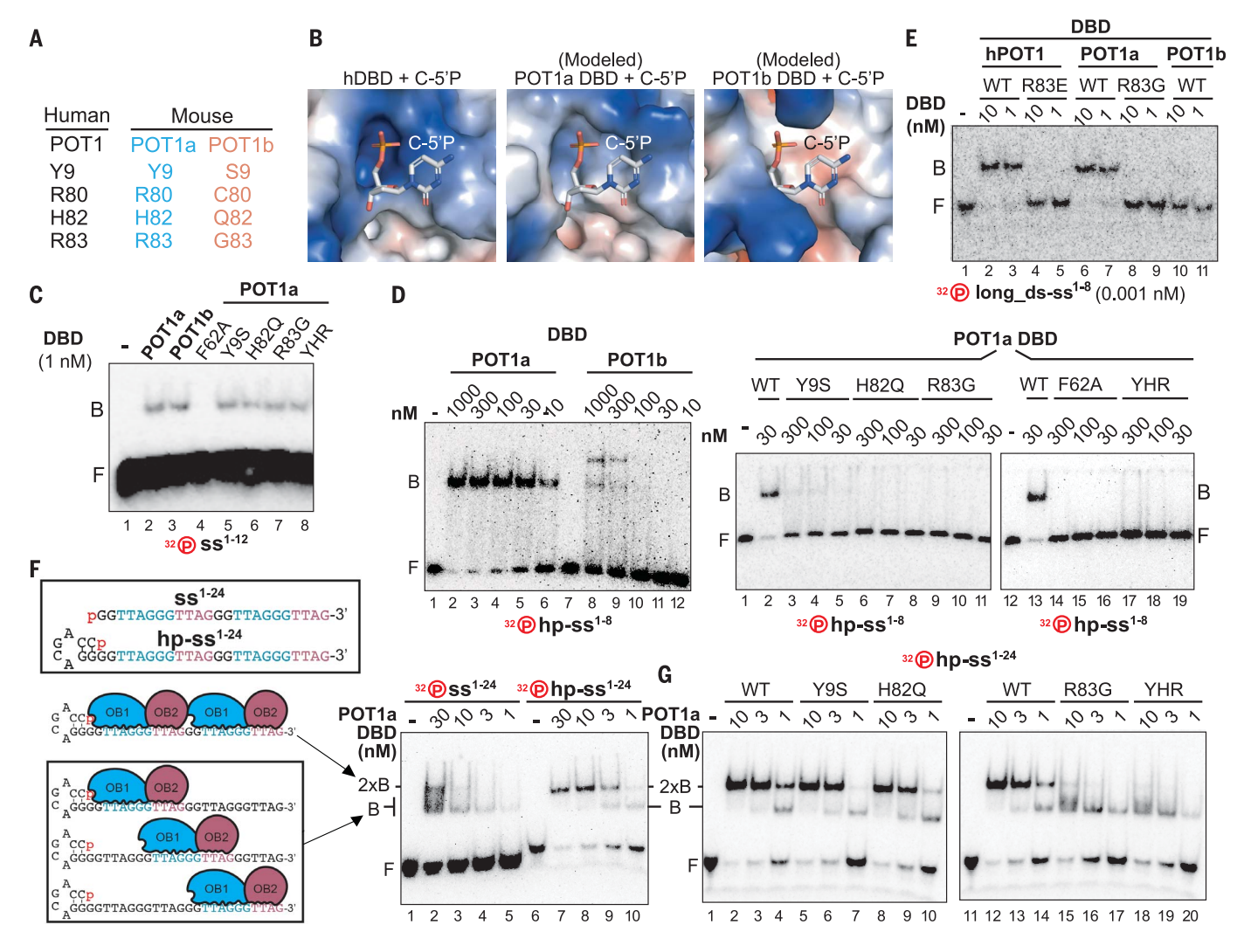


Fig. 4. Presence of the POT-hole dictates POT1 paralog choice for chromosome-end protection in mice. (A) Human POT-hole residues are conserved in mouse POT1a but not mouse POT1b. (B) Electrostatic surface comparisons of hDBD (from hDBD-5'-P-ds-ss¹⁻¹² structure) and POT1a and POT1b DBD (Alphafold models), with the phosphorylated 5'-C of the hDBD-bound structure shown in sticks. (**C** and **D**) EMSA analysis of indicated mouse POT1a and POT1b DBD constructs with the indicated 5'- 32 P-labeled oligonucleotides [0.1 nM for (C) and (D), right; 0.01 nM for (D), left]; n = 3. (**E**) EMSA analysis of indicated human and mouse POT1 DBD constructs with 0.001 nM 5'- 32 P-long_ds-ss¹⁻⁸

two-stranded DNA; n=3. (**F**) (Top left) Names and sequences of the two DNA oligonucleotides, hp-ss¹⁻²⁴ and ss¹⁻²⁴, used to evaluate 5'-end-binding preference. Both DNAs were labeled at the 5' end with ³²P for EMSA analysis. (Bottom left) Three possible DNA-binding registers for the first DBD molecule are shown with the center-binding register precluding the binding of a second DBD molecule. (Right) EMSA analysis of POT1a DBD with hp-ss¹⁻²⁴ (discrete slow-migrating band with increasing concentrations of protein; 2×B) and ss¹⁻²⁴ (smeary band; mixture of B and 2×B), DNA at 0.1 nM; n=3. (**G**) EMSA analysis of indicated POT1a DBD constructs with 0.1 nM hp-ss¹⁻²⁴. YHR, triple mutant Y9S-H820-R83G; n=3.

being critical for both DNA-binding modes. These data highlight the importance of the POT-hole in 5'-end binding and provide separation-of-function mutants to test the importance of hPOT1's junction-binding activity in cells (Fig. 3B).

Loss of POT1 binding at the 3' overhang results in telomere dysfunction-induced foci (TIF), which signify the recognition of telomeres by the DDR machinery (33). To determine the biological importance of the POT-hole binding to the telomeric junction, we used a previously described cell line in which POT1 can be deleted

in an inducible fashion (*POTI* KO) (*34*) to test the ability of transduced WT and mutant hPOTI Myc-tagged constructs to compensate for the loss of endogenous POT1 (materials and methods). Transduced cells were treated first with 4-OHT to delete *POTI* and then either treated with doxycycline (dox) to induce exogenous hPOT1 expression ("+dox") or left untreated ("-dox") (Fig. 3C). In the absence of dox, 4-OHT treatment resulted in a robust TIF phenotype, characterized by colocalization of the DDR factor 53BP1 at telomeres (fig. S6, E and F). hPOT1 wild type and "low dox" wild

type, but not hPOT1 F62A, suppressed TIFs (Fig. 3, D and E). POT-hole mutants Y9A, R83A, and R83E were defective in TIF suppression compared with wild type, with R83E being the most deleterious (Fig. 3, D and E). This trend emphasizes the importance of the ionic interaction between R83 and the 5'-P. Clones isolated from 6X-Myc-tagged hPOT1 WT, F62A, and R83E cell populations also recapitulated the TIF phenotypes (fig. S7, A to D). Furthermore, TIFs were smaller (Fig. 3D, inset) and less frequent (Fig. 3, D and E) in POT-hole mutant cells compared with those in F62A

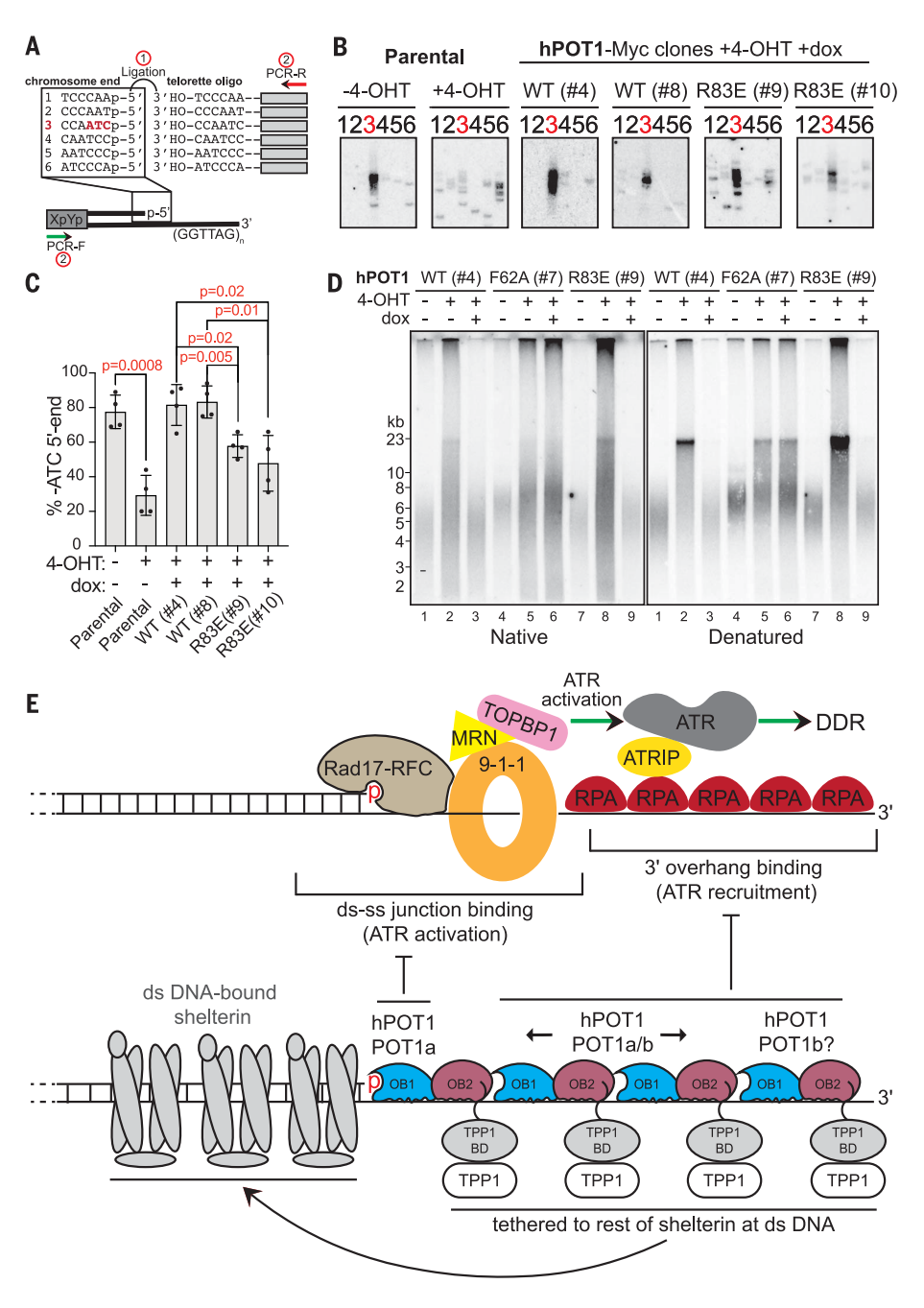


Fig. 5. Maintenance of the ATC-5' end of chromosomes by the POT-hole. (A) Schematic of the modified STELA technique for determining the chromosomal 5'-terminal nucleotide in human cell lines. Step 1: DNA ligation of genomic DNA 5'-P ends with telorettes ending in each of the six possible repeat registers at the 3'-OH ends. Step 2: PCR amplification of the ligation products performed with a forward primer (PCR-F) targeting the subtelomere of chromosome XpYp and a reverse primer (PCR-R) targeting a sequence shared by all telorettes. The products are visualized with Southern blot analysis performed with a 5'-32P-labeled XpYpB2 reverse primer. (B) STELA-based determination of the chromosomal 5'-terminal nucleotide in the HEK 293E-based POT1 KO parental cell line (-4-OHT and +4-OHT) and hPOT1-Myc WT- or R83Ecomplemented clonal cell lines treated with both 4-OHT and dox. (C) Ouantitation of ATC-5' preference calculated as the ratio of the total band intensity in the primer 3 lane over the total intensity over all six lanes. Mean and SD for n = 4 replicates of which B is representative are plotted. P values were calculated with a two-tailed Student's t test for comparisons against parental -4-OHT data (for parental +4-OHT) or hPOT1-Myc WT clones (for hPOT1-Myc R83E clones). (D) (Left) TRF analysis of cell lines used in (B) performed first under native conditions with a 5'-32P-labeled telomeric C-probe (CTAACC)₄ to detect the ss G-rich overhang. (Right) TRF analysis after denaturing the DNA on the same gel and reprobing it to detect the total telomeric DNA signal; n = 1. (**E**) Model for ATR inhibition at telomeres by POT1. The ssDNAbinding of hPOT1 prevents the loading of RPA to curb ATR recruitment to the 3' overhang. Protection of the ds-ss junction by hPOT1 prevents loading of the 9-1-1/Rad17-RFC clamp and clamp-loader complex and ATR activator TOPBP1. In mice, both POT1 paralogs coat the ss overhang, but only POT1a protects the ds-ss junction. The shelterin proteins protecting the telomeric dsDNA are expected to keep POT1-TPP1 tethered to the ss overhang, facilitated by protein-protein interactions and the conformational flexibility within the proteins (29) and the telomeric DNA.

cells. This finding suggests that both junctionand ssDNA-binding activities of hPOT1 must be compromised to trigger a full DDR (see Discussion). Our results demonstrate that junction binding, which should involve a single POT1 molecule per chromosome end (Fig. 3B), is critical for chromosome-end protection.

The POT-hole differentiates mouse POT1 paralogs and enables POT1a to protect the telomeric junction

Despite being strictly conserved in other mammalian POT1 homologs, including mouse POT1a,

each of the four POT-hole amino acids is replaced with a structurally disparate residue in mouse POT1b (Fig. 4A and fig. S8A). By contrast, the residues used in ss DNA binding are conserved in all mammalian POT1 homologs, including POT1b (fig. S8A). Aligning Alphafold predictions (35) of POT1a and POT1b DBDs with the junction-bound structure of hDBD illustrates that the shape and electropositive nature of the POT-hole are predicted to be lost in POT1b (Fig. 4B and fig. S8, B and C). We hypothesized that POT1a, but not POT1b, protects the 5' end at the junction. Indeed, POT1a-

and POT1b-DBD proteins bound ss¹⁻¹², but only POT1a DBD engaged a telomeric ds-ss junction with high affinity (Fig. 4, C to E, and fig. S8, D and E). POT1a replaced with POT1b residues in the POT-hole (except R80; fig. S8F legend explains rationale) retained affinity toward ss¹⁻¹² (Fig. 4C) but failed to bind the junction (Fig. 4D, right, and E, and fig. S8D).

To measure junction-binding in the presence of multiple ss DNA-binding sites, we developed an EMSA-based "POT1 packing" assay with two DNA targets, each containing four telomeric ss repeats (24 nt) spanning three possible

POT1-binding registers. The 5' and 3' registers are compatible with the packing of two POT1 molecules, whereas binding to a central register precludes the loading of a second POT1 (Fig. 4F, left). hp-ss¹⁻²⁴ includes a ds-ss junction upstream of this ss region, whereas ss1-24 does not. A fully packed 2:1 DBD-DNA complex would produce a sharp, slow-migrating band at higher DBD concentrations, whereas a mix of 2:1 and 1:1 complexes (of various binding registers) would generate a smear. POTIa DBD binding resulted in a sharp band for hp-ss1-24 but not ss¹⁻²⁴, suggesting that the protein packs preferentially against a ds-ss junction but that there is no end-binding bias to dissuade it from binding to the central site of ss¹⁻²⁴ (Fig. 4F. right). POT1a POT-hole mutants R83G and triple mutant YHR lost the ability to pack at the junction (Fig. 4G), which is consistent with R83 capping the 5' terminus (Fig. 2, D and F) and repressing TIFs (Fig. 3, D and E). hDBD and mouse POT1b DBD formed a discrete complex with not only hp-ss1-24 but also ss1-24, which is consistent with a 3'-end-binding preference (fig. S9, A and B) (7). Our results demonstrate that the POT-hole allows POT1a to preferentially bind the telomeric junction.

The POT-hole helps maintain the 5'-end identity of human chromosomes

Consistent with the structures we solved, the POT-hole of hDBD and mouse POTIa DBD protect the 5'-P end from 5' exonucleolytic action in vitro (fig. S10, A to F). We next asked whether the POT-hole helps maintain the 5'-terminal sequence of the chromosomes in cells. We used a modified single telomere length analysis (STELA) approach that uses ligation-mediated polymerase chain reaction (PCR) amplification to determine the abundance of each of the six possible chromosomal 5'-end permutations (Fig. 5A) (23). Genomic DNA extracted from the parental human embryonic kidney (HEK) 293E cell line displayed the expected ATC-5' preference that is lost after POT1 deletion (Fig. 5, B and C). WT hPOT1, but not R83E hPOT1, was able to restore the ATC-5' bias to untreated (parental -4-OHT) levels, demonstrating that the POT-hole helps maintain the 5' end of the human chromosome (Fig. 5, B and C, and fig. S10G). The 5'-end scrambling of hPOT1 R83E was less severe than that of POT1 KO. This difference may be explained by the unleashing of 5' exonuclease activity at telomeres completely devoid of POT1 (36). Terminal restriction fragment (TRF) analysis reproduced previously characterized phenotypes (15, 34, 37), including the accumulation of slow-migrating species (denatured and native blots) and an increase in the G-rich ss signal (native blot) upon POT1 deletion, which were suppressed by expression of hPOT1 wild type but not F62A (Fig. 5D and fig. S10H). R83E recapitulated the WT phenotypes, suggesting that the end-protection function of the POT-hole is separable from hPOTI's role in bulk-telomere or overhang-length maintenance. Thus, the POT-hole helps maintain ATC-5' ends without acutely influencing telomere length.

Discussion

The major pathway of ATR activation requires RPA binding to exposed ssDNA and recognition of the ds-ss junction by the 9-1-1/Rad17-RFC (RAD9-RAD1-HUS1/Rad17-RFC2-RFC3-RFC4-RFC5) clamp and clamp loader, which with the MRN (MRE11-RAD50-NBS1) complex recruit TOPBP1 (DNA topoisomerase 2-binding protein 1) to activate ATR (Fig. 5E) (4, 38). The structure of human 9-1-1/Rad17-RFC bound to a ds-ss junction revealed a basic pocket in Rad17 that is poised to bind the 5'-phosphorylated end of a junction by using a mechanism similar to that of POT1 (fig. S11, A and B) (39). Consistent with a competition between POT1 and 9-1-1/Rad17-RFC in binding the ds-ss junction, subunits of the 9-1-1 and MRN complexes, as well as TOPBP1, are enriched at telomeres in the absence of hPOT1 (34). We therefore propose that POT1 not only outcompetes RPA at the telomeric ss overhang but also prevents ATR activation by denying 9-1-1/Rad17-RFC access to the telomeric ds-ss iunction (Fig. 5E).

The duplication of POT1 (40), the conservation of the POT-hole in POT1a (fig. S12A), the disruption of the POT1-hole in POT1b (fig. S12B), and the retention of CTC1-STN1-TEN1 (CST)-binding motifs in POT1b (40) within the Muridae and Cricetidae families of the Rodentia order provide support to the hypothesis that POT1b relinquished junction binding to facilitate processes at the 3' end. We propose that POT1a wards off 9-1-1/Rad17-RFC at the junction, although both POT1a and POT1b paralogs could counter RPA at the overhang in mouse cells (Fig. 5E).

The POT-hole is conserved in species distant to mammals, such as Sterkiella nova and Caenorhabditis elegans (fig. S13A). The precisely defined S. nova macronuclear telomere contains a 5'-C at the ds-ss junction and a 16-nt overhang that binds one telomere end-binding protein (TEBP)α/β complex (homologous to the POT1-TPP1 complex) (41). TEBPα has been crystallized with a sulfate ion bound in a manner indistinguishable from how the 5'-P binds hDBD in our junction-bound structures (fig. S13B) (42). Indeed, like hPOT1, TEBP α binds the telomeric ds-ss junction more strongly than it binds telomeric ssDNA (8). These observations point to a single TEBPα/β complex simultaneously protecting the 5' and 3' ends of the chromosome (8, 41, 42). Schizosaccharomyces pombe, in which a POT-hole is not obvious (fig. S13, A and C) (5, 43), and eukaryotes whose chromosomes do not end in a 5'-C, must have evolved alternative approaches for junction protection.

We updated the model for how telomeres avert detection by the DDR machinery to include a critical role of POT1 in binding the telomeric ds-ss junction. Thus, POT1 protects both DNA strands at human chromosome ends by coating the G-rich ss overhang and recognizing the phosphorylated 5' end of the C-rich strand.

REFERENCES AND NOTES

- 1. W. Palm, T. de Lange, Annu. Rev. Genet. 42, 301-334 (2008).
- 2. F. L. Denchi, T. de Lange, *Nature* **448**, 1068–1071 (2007).
- 3. T. de Lange, Annu. Rev. Genet. 52, 223-247 (2018).
- J. C. Saldivar, D. Cortez, K. A. Cimprich, Nat. Rev. Mol. Cell Biol. 18, 622–636 (2017).
- P. Baumann, T. R. Cech, Science 292, 1171–1175 (2001).
- 6. Y. Gong, T. de Lange, Mol. Cell 40, 377-387 (2010).
- M. Lei, E. R. Podell, T. R. Cech, Nat. Struct. Mol. Biol. 11, 1223–1229 (2004).
- 8. D. E. Gottschling, V. A. Zakian, Cell 47, 195-205 (1986).
- 9. C. M. Price, T. R. Cech, Genes Dev. 1, 783-793 (1987).
- M. P. Horvath, V. L. Schweiker, J. M. Bevilacqua, J. A. Ruggles, S. C. Schultz, *Cell* **95**, 963–974 (1998).
- C. I. Nugent, T. R. Hughes, N. F. Lue, V. Lundblad, Science 274, 249–252 (1996).
- J. J. Lin, V. A. Zakian, Proc. Natl. Acad. Sci. U.S.A. 93, 13760–13765 (1996).
- 13. M. Raices et al., Cell 132, 745-757 (2008).
- 14. L. Wu et al., Cell **126**, 49–62 (2006).
- D. Hockemeyer, J. P. Daniels, H. Takai, T. de Lange, *Cell* 126 63–77 (2006).
- K. Kratz, T. de Lange, J. Biol. Chem. 293, 14384–14392 (2018).
 W. Palm, D. Hockemeyer, T. Kibe, T. de Lange, Mol. Cell. Biol.
- W. Palm, D. Hockemeyer, T. Kibe, T. de Lange, Mol. Cell. Biol. 29, 471–482 (2009).
- 18. P. Gu et al., Nat. Commun. 12, 5514 (2021).
- 19. L. Y. Chen, S. Redon, J. Lingner, Nature 488, 540-544 (2012).
- P. Wu, H. Takai, T. de Lange, *Cell* **150**, 39–52 (2012).
 M. Wan, J. Qin, Z. Songyang, D. Liu, *J. Biol. Chem.* **284**,
- M. Wan, J. Qin, Z. Songyang, D. Liu, J. Biol. Chem. 28-26725–26731 (2009).
- D. Hockemeyer, A. J. Sfeir, J. W. Shay, W. E. Wright, T. de Lange, *EMBO J.* 24, 2667–2678 (2005).
- A. J. Sfeir, W. Chai, J. W. Shay, W. E. Wright, Mol. Cell 18, 131–138 (2005).
- 24. K. H. Choi et al., Biochimie 115, 17-27 (2015).
- D. M. Baird, J. Rowson, D. Wynford-Thomas, D. Kipling, Nat. Genet. 33, 203–207 (2003).
- C. J. Lim, A. J. Zaug, H. J. Kim, T. R. Cech, Nat. Commun. 8, 1075 (2017).
- T. Paul, W. Liou, X. Cai, P. L. Opresko, S. Myong, *Nucleic Acids Res.* 49, 12377–12393 (2021).
- S. Ray, J. N. Bandaria, M. H. Qureshi, A. Yildiz, H. Balci, *Proc. Natl. Acad. Sci. U.S.A.* 111, 2990–2995 (2014).
- J. C. Zinder et al., Proc. Natl. Acad. Sci. U.S.A. 119, e2201662119 (2022).
- 30. F. Wang et al., Nature **445**, 506–510 (2007).
- 31. J. Nandakumar et al., Nature 492, 285-289 (2012).
- 32. H. He et al., EMBO J. 25, 5180-5190 (2006).
- 33. H. Takai, A. Smogorzewska, T. de Lange, *Curr. Biol.* **13**, 1549–1556 (2003).
- 34. G. Glousker, A. S. Briod, M. Quadroni, J. Lingner, *EMBO J.* **39**, e104500 (2020).
- 35. J. Jumper et al., Nature 596, 583-589 (2021).
- T. Kibe, M. Zimmermann, T. de Lange, Mol. Cell 61, 236–246 (2016).
- 37. D. Loayza, T. De Lange, Nature 423, 1013-1018 (2003).
- 38. C. A. MacDougall, T. S. Byun, C. Van, M. C. Yee, K. A. Cimprich, *Genes Dev.* **21**, 898–903 (2007).
- M. Day, A. W. Oliver, L. H. Pearl, *Nucleic Acids Res.* 50, 8279–8289 (2022).
- 40. L. R. Myler et al., Genes Dev. 35, 1625-1641 (2021).
- L. A. Klobutcher, M. T. Swanton, P. Donini, D. M. Prescott, Proc. Natl. Acad. Sci. U.S.A. 78, 3015–3019 (1981).
- S. Classen, J. A. Ruggles, S. C. Schultz, J. Mol. Biol. 314, 1113–1125 (2001).
- M. Lei, E. R. Podell, P. Baumann, T. R. Cech, *Nature* 426, 198–203 (2003).

ACKNOWLEDGMENTS

We thank S. Padmanaban (Nandakumar laboratory) for input on the design of the cell-based experiments; G. Glousker and J. Lingner [Ecole Polytechnique Fédérale de Lausanne (EPFL),

Switzerland] for graciously gifting the POT1-inducible KO HEK 293E cell line and the pCW22 TREtight MCS UBC rtTA IRES Blast lentiviral vector for dox-inducible expression and for sharing detailed protocols and troubleshooting tips for these resources; J. Schmidt (Michigan State University, USA) for the 53BP1 antibody; the beamline staff at the Life Sciences Collaborative Access Team (LS-CAT) beamline of the Argonne National Laboratory for help with x-ray diffraction data collection [use of the Advanced Photon Source, an Office of Science User Facility operated for the US Department of Energy (DOE) Office of Science by Argonne National Laboratory, was supported by the US DOE under contract no. DE-AC02-06CH11357]; F. C. Lowder and L. Simmons (University of Michigan at Ann Arbor, USA) for helpful suggestions for the exonuclease protection experiment carried out with fluorophorelabeled DNA and for preparation of an RNA ladder; T. de Lange and S. Cai (Rockefeller University, USA), J. Schmidt (Michigan State University, USA), H. Shibuya (University of Gothenburg, Sweden),

and J. Williams (Nandakumar laboratory) for helpful comments on the manuscript; and G. Sobocinski for help with microscopy. Funding: This study was supported by NIH grants R01GM120094, R01HD108809, and R35GM148276 (J.N.) and by American Cancer Society Research Scholar grant RSG-17-037-01-DMC (J.N.). Author contributions: Conceptualization: V.M.T. and J.N. Methodology: V.M.T., K.A.B., and J.N. Investigation: V.M.T. and K.A.B. Visualization: V.M.T., K.A.B., and J.N. Funding acquisition: J.N. Project administration: V.M.T. and J.N. Supervision: V.M.T. and J.N. Writing - original draft: V.M.T. and J.N. Writing - review and editing: V.M.T., K.A.B., and J.N. Competing interests: The authors declare that they have no competing interests. Data and materials availability: All data are available in the main and supplementary figures. All material generated in this study, such as plasmids for protein expression and cell lines, are available upon request. Coordinates and structure factors of the crystal structures of hDBD with 5'-P-hp-ss1-12 and 5'-Pds-ss¹⁻¹² are deposited in the Protein Data Bank (PDB) under

accession codes 8SH0 and 8SH1, respectively. **License information:** Copyright © 2023 the authors, some rights reserved; exclusive licenses American Association for the Advancement of Science. No claim to original US government works. https://www.science.org/about/science-licenses-journal-article-reuse

SUPPLEMENTARY MATERIALS

science.org/doi/10.1126/science.adi2436 Materials and Methods Figs. S1 to S13 Tables S1 and S2 References (44–55) MDAR Reproducibility Checklist

Submitted 19 April 2023; accepted 19 July 2023 10.1126/science.adi2436

Tesmer et al., Science **381**, 771–778 (2023) 18 August 2023 **8 of 8**